Hindawi Publishing Corporation
Journal of Nanomaterials
Volume 2015, Article ID 589754, 9 pages
http://dx.doi.org/10.1155/2015/589754

Research Article

Microstructure and Mechanical Properties of Multiphase Strengthened Al/Si/Al_2O_3/SiO_2/MWCNTs Nanocomposites Sintered by *In Situ* Vacuum Hot Pressing

Jingrui Li,[1] Xiaosong Jiang,[1] Zhenyi Shao,[2] Degui Zhu,[1] Shardai S. Johnson,[3] Zhiping Luo,[3] and Minhao Zhu[1]

[1]*School of Materials Science and Engineering, Southwest Jiaotong University, Chengdu, Sichuan 610031, China*
[2]*School of Materials Engineering, Chengdu Technological University, Chengdu, Sichuan 611730, China*
[3]*Department of Chemistry and Physics, Fayetteville State University, Fayetteville, NC 28301, USA*

Correspondence should be addressed to Xiaosong Jiang; xsjiang@home.swjtu.edu.cn and Zhiping Luo; zluo@uncfsu.edu

Received 3 September 2015; Revised 8 November 2015; Accepted 17 November 2015

Academic Editor: Albert Nasibulin

Eutectic Al–Si binary alloy is technically one of the most important Al casting alloys due to its high corrosion resistance, evident shrinkage reduction, low thermal expansion coefficient, high fluidity, and good weldability. In this work, multiphased Al–Si matrix nanocomposites reinforced with Al_2O_3 and multiwalled carbon nanotubes (MWCNTs) have been sintered by an *in situ* vacuum hot-pressing method. The alumina Al_2O_3 nanoparticles were introduced by an *in situ* reaction of Al with SiO_2. Microstructure and mechanical properties of the sintered Al/Si/Al_2O_3/SiO_2/MWCNTs nanocomposites with different alumina contents were investigated. The mechanical properties were determined by micro-Vickers hardness and compressive and shear strength tests. The results demonstrated that *in situ* alumina and MWCNTs had impacts on microstructure and mechanical properties of the nanocomposites. Based on the mechanical properties and microstructure of the nanocomposites, strengthening and fracture mechanisms by multiple reinforcements were analyzed.

1. Introduction

Aluminum-matrix composite materials have found wide applications in aerospace, transportation, sports, defense, and other fields, owing to their low mass densities, high specific strengths, good impact resistance, high temperature resistance, durable wear resistance, and other exceptional properties [1–5]. Al–Si binary alloy, in a simple eutectic system, is one of the most important Al casting alloys since Si acts as a bridge to connect the matrix and reinforcements with improved bindings. Various particles, whiskers, and fibers have been used as reinforcements in Al-matrix composites. Among them, Al_2O_3 alumina particles and carbon nanotubes (CNTs) have been widely used to improve the composite mechanical properties as follows.

(1) Al_2O_3 particle reinforcements: Dash et al. studied effect of different volume fraction of micron level and nanosized alumina particles on the performance of Al-matrix composites by using spark plasma sintering technique [6]. Further, relationship between intensity or damping performance and temperature was discussed by Casati et al. through preparation of nano alumina-reinforced Al-matrix nanocomposites by means of high-energy ball milling and powder metallurgy method, combined with hot and cold extrusion molding process [7]. On the other hand, it was found by Jiang et al. that *in situ* synthesized Al_2O_3 particles could enhance wear and mechanical properties of Al_2O_3 reinforced Al-matrix composites, with better performance than that of directly participated Al_2O_3 [8]. Generally, the products by *in situ* synthesis can overcome some shortcomings of the conventional methods, such as poor compatibility and interfacial pollutions.

(2) Multiwalled carbon nanotube (MWCNT) reinforcements. MWCNTs are ideal composite reinforcements

because of their high mechanical strengths, desirable flexibilities, low thermal expansion coefficient, and other small-size enhanced properties [9–11]. Studies have shown that mechanical performances of CNT-reinforced Al-matrix composites are superior to other traditional filler reinforced Al-matrix composites. However, because of their large specific surface areas, high surface energies, and great Van der Waals forces, MWCNTs tend to agglomerate and it is normally hard to evenly disperse them into the metal matrix [11–13]. However, it is well known that the dispersion is critically important to composite materials, as it dominates the materials' properties [14, 15]. Surface modifications will be conducted to achieve good dispersion of MWCNTs in this work.

In the open literature, most of the experiments on the nanocomposites focus on single or limited number of reinforcements. However, the enhancement by a single reinforcement sometimes does not fully meet the requirements for the composite, while multiphases should be introduced, as reported by some researchers [16–18]. Considering the alumina Al_2O_3 and MWCNTs, two types of reinforcements, since Al_2O_3 particles are hard and rigid while MWCNTs are flexible at the nanoscale, when they are introduced to the Al–Si matrix, they may produce synergistic cooperative and multiscale reinforcements.

In this work, we attempt to prepare Al composites with both Al_2O_3 and MWCNTs two components by a vacuum hot-pressing method. SiO_2 particles were added for *in situ* synthesis of Al_2O_3 particles to achieve multiple phases. Mechanical properties of the nanocomposites were measured to evaluate their reinforcing effects. Based on the experimental results, the strengthening and fracture mechanisms of the nanocomposites with multiple phases were discussed.

2. Experimental Procedures

Based on the concept of multiphase reinforcements for enhanced effect, we used a powder metallurgy method to sinter the nanocomposites by *in situ* vacuum hot pressing. Such a powder metallurgy method worked at a preparation temperature which is much lower than the traditional methods to prevent a product of brittle Al_4C_3 interfacial phase [19].

Raw materials of Al, SiO_2, and MWCNTs powders were used, with their specifications listed in Table 1. During the hot pressing, replacement reaction between Al and SiO_2 occurred as follows:

$$4Al + 3SiO_2 \longrightarrow 3Si + 2Al_2O_3 \quad (1)$$

The reaction product Al_2O_3 acts as reinforcements in the matrix, and the other product Si forms Al–Si alloy with the matrix. Al_2O_3 particles, Si, and MWCNTs have different enhancements to the Al matrix to improve the mechanical properties. Gibbs free energy state function can be used to determine whether a chemical reaction can occur spontaneously. The Gibbs standard-state free energy is expressed as

$$\Delta G_T^0 = \Delta H_T^0 - T\Delta S_T^0 \quad (2)$$

Table 1: Properties of raw material powders.

Material	Size	Purity (%)
Al	26–30 μm	≥99.7
SiO_2	≤13 μm	≥99.9
MWCNTs	Diameter 20–30 nm, length 10–30 μm	≥95

Here, ΔH is molar reaction enthalpy, ΔS is molar reaction entropy, and T stands for temperature. The ΔG_T^0 is calculated to be −569.6 kJ/mol and −534.4 kJ/mol for temperature T at 600 K and 1000 K, respectively. If $\Delta G_T^0 < 0$, the reaction occurs in thermodynamics. Under the experimental conditions, reaction (1) is possible.

In order to achieve a good dispersion of MWCNTs, noncovalent and covalent surface modifications of MWCNTs were prepared using 10 μg/mL gallic acid aqueous solutions [20, 21]. The raw powders in the weight ratio of $Al : SiO_2 : MWCNTs = 9.470 : 1.000 : 0.268$, respectively, were mixed by high-energy ball milling for 1 h and then were placed in a hot-press chamber and heated from room temperature to 900 K under a pressure of 61.1 MPa applied on the powders. The experimental temperature is determined by the Al–Si eutectic point (850 K) and the chemical reaction in this system. Low-pressure sintering produces higher porosities, and low-temperature sintering yields samples with lower properties, due to the limited *in situ* reactions. However, higher pressure or higher temperature may cause leak of the Al melt during the process. The content of MWCNTs in the mixed powders is 2.5 wt-%. After holding the pressure for 30 min, the pressure was released and the sample was kept at the same high temperature for a period of sintering time of 2 h or 8 h, respectively. The furnace was then naturally cooled to room temperature. The microstructure of the nanocomposites was studied by X-ray diffraction (XRD, X'Pert Pro-MPD) analysis, scanning electron microscope (SEM, JEOL JSM-7001F at 15 kV), and transmission electron microscope (TEM, FEI Tecnai F20ST at 200 kV), both equipped with X-ray energy-dispersive spectrometer (EDS) and electron probe microanalyzer (EPMA, JEOL JXA-8530F field-emission hyperprobe at 15 kV) for elemental mapping using wavelength-dispersive spectrometer (WDS). The sample for TEM was prepared by ion milling, and the samples for EPMA were embedded in epoxy resin and polished and coated with carbon layers to achieve surface conductivity. The hardness measurements were carried out using a micro-Vickers hardness tester (HXD-100TM/LCD). The test load was 100 kgf, and the loading and dwell time WERE 8 s and 15 s, respectively. Shear and compression tests were performed using a microcomputer-controlled electronic universal testing machine (WDW-3100) at a loading rate of 0.5 mm/min.

3. Results and Discussion

3.1. Microstructure and Phase Identification. The SEM images of Al, SiO_2, and MWCNTs powders after ball milling are shown in Figure 1. The larger particles are Al, and the smaller

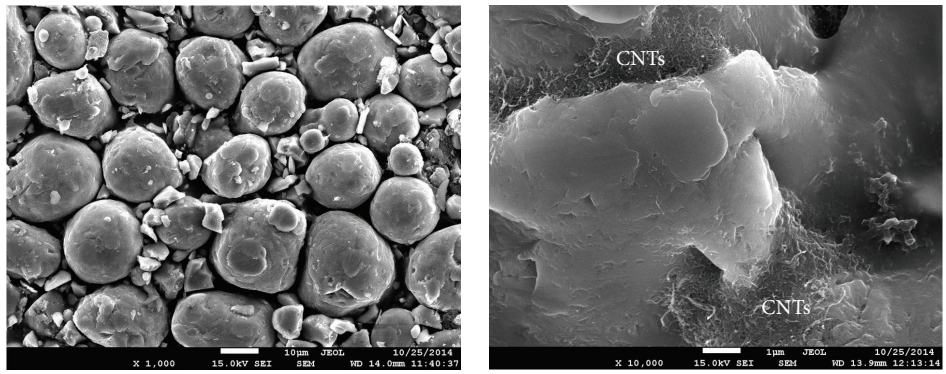

(a) (b)

FIGURE 1: SEM images of raw materials of Al, SiO_2, and MWCNTs after ball milling, taken at a low magnification (a) and a high magnification (b).

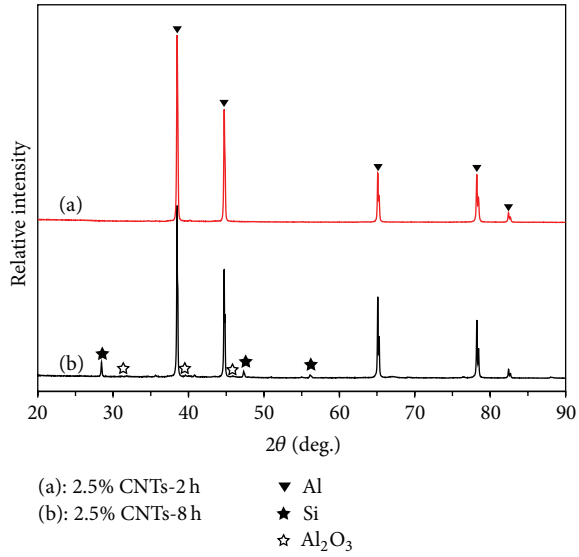

FIGURE 2: XRD patterns of sintered nanocomposites with sintering time of 2 h and 8 h, respectively.

particles are SiO_2 which are uniformly dispersed between Al particles (Figure 1(a)). At a higher magnification, MWCNTs are found dispersed on the periphery surfaces of Al and SiO_2 particles, as shown in Figure 1(b). The mixed powders were sintered by vacuum hot pressing at 900 K under a pressure of 61.1 MPa to obtain Al-matrix nanocomposite. Figure 2 shows the XRD patterns of the nanocomposites prepared with two periods of sintering time of 2 h and 8 h, respectively. By using 2 h sintering time, as shown in Figure 2(a), no evident reaction between Al and SiO_2 is found. The pattern only exhibits Al phase, while the small SiO_2 and MWCNTs do not show up in the pattern. However, when the sintering time is extended to 8 h, two products of Al_2O_3 and Si are present in the pattern, as shown in Figure 2(b). No reactant of Al_4C_3 phase was detected in the XRD patterns.

To further identify the products, the microstructure of nanocomposite sintered by 8 h is analyzed in EPMA for elemental mapping. As shown in Figure 3(a), the backscattered (BS) image shows clearly Al grains in a higher contrast, while SiO_2 locates between Al grains in a darker contrast. The mass density of Al (2.7 g/cm^3) is higher than SiO_2 (2.65 g/cm^3), so Al exhibits a higher intensity over SiO_2 in the BS image. It is noticed that the Al grain size is significantly reduced as compared with the raw Al grains in 26–30 μm. The averaged grain size is measured as 4.7 μm, with a standard deviation of 2.0 μm. Apparently, the Al grains are refined in the product. Since the eutectic temperature of Al–Si alloy is 850 K which is lower than the processing temperature of 900 K, partial melting of the Al grains is possible to form the smaller Al grains based on the increased preferable nucleation sites of the foreign enforcements. The Al map, collected by WDS, is shown in Figure 3(b). The Al grain central regions exhibit red-orange color, indicating higher Al concentrations. It is found that the Al grains are covered with layers in green color, indicating a lower Al concentration as compared with pure Al, possibly by the formation of Al_2O_3 on the surfaces or the diffusion of Al into the SiO_2 regions to lower down the Al concentration. The areas of the SiO_2 still exhibit blue color, while such signals could come from the Al matrix underneath due to the large interaction volume of the electron beam with the bulk specimen. The O and Si maps are shown in Figures 3(c) and 3(d), respectively. It is evident that the O regions are widened as compared with the Si regions, implying that O has diffused away from the original SiO_2 locations. Some dispersed Al_2O_3 particles can be found in the Al grains in Figure 3(c), in a higher contrast as indicated by some arrows.

In the SEM image, as shown in Figure 4(a), it is found that white particles are uniformly dispersed in the matrix, without the presence of Al_4C_3 plates. Some small pores are also observed, due to the incomplete densification of the composite prepared by the powder metallurgy method. As shown in the magnified image in Figure 4(b), the white particle is identified as the reinforcing phase of Al_2O_3, with the presence of small SiO_2 particles, as a remaining phase of the reaction (1), in the center appearing in a darker contrast. The EDS measurements in Figures 4(c) and 4(d) confirm the Al_2O_3 and SiO_2 compositions, respectively.

TEM image of the prepared nanocomposite is shown in Figure 5(a). High-density dislocations can be found in the

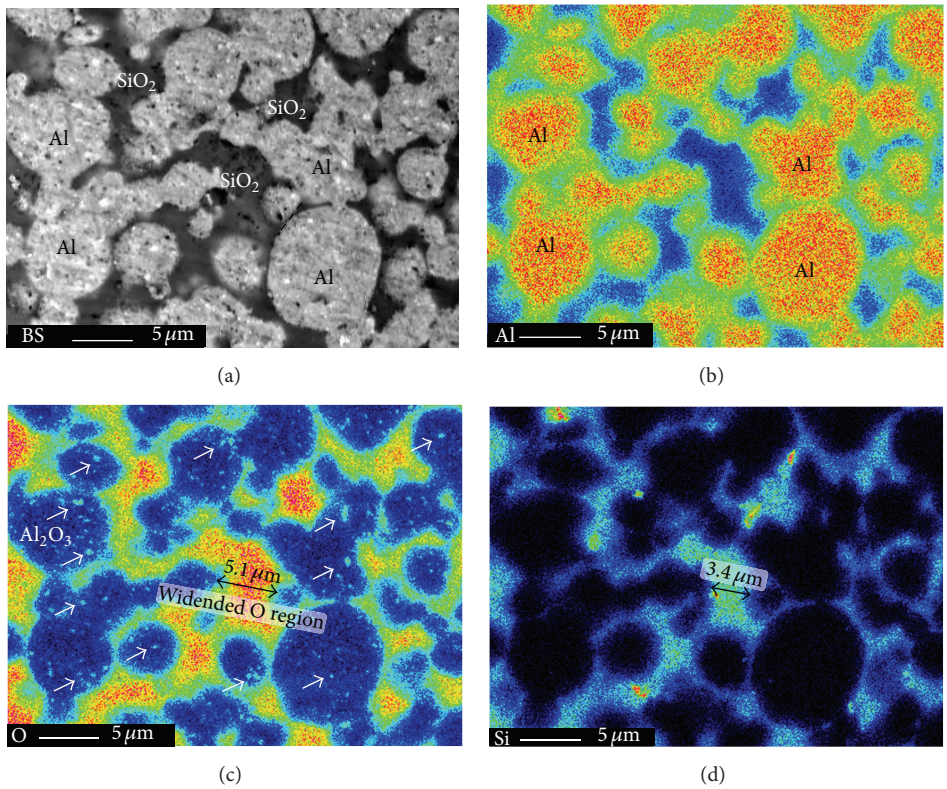

Figure 3: EPMA analyses of sintered nanocomposites with 8 h sintering time. (a) BS image; (b) Al map; (c) O map; (d) Si map.

Al matrix near the lower-right side, while alumina particles, as confirmed by EDS, are found at upper-left side. From Figure 5(a), it is apparent that the alumina particles blocked the dislocations in Al matrix. An electron diffraction pattern from Al is inserted in the figure, confirming Al face-centered cubic structure. An enlargement of the alumina particles is shown in Figure 5(b), indicating that the product of alumina is indeed composed of small nanoparticles.

These observations indicated that *in situ* reactions happened during the hot pressing, although small amount of SiO_2 particles remained. However, this reaction process involved an inoculation period and a reaction period. As the reaction starts, the Al atoms contact and react with SiO_2 during the inoculation period, as the Al is liable to be oxidized. On the surface when a thin layer of Al_2O_3 particles is formed, the alumina particles impede the direct contact between Al atoms and SiO_2. Thus, with a short sintering time (2 h), no evident reaction products are found, whereas, with extended sintering time of 8 h, the Al atoms could diffuse to penetrate the Al_2O_3 regions, extending the reaction inoculation period [22]. The *in situ* reaction started in the course of time. The alumina generated during reaction diffuse inward and thus the size of the remaining SiO_2 particles become smaller and smaller, while the Al_2O_3 layer is gradually thickened. On the other hand, research has indicated that addition of carbon increased the apparent activation energy of the *in situ* reaction. The carbon in the vicinity of the reactant particles reduces the contact between reactants to hinder the reaction [23]. The substance migration and diffusion between solid-phase particles require a longer sintering time with the presence of carbon.

3.2. Hardness Measurements of the Nanocomposites. The results of micro-Vickers hardness are listed in Table 2. The average hardness of the nanocomposite sintered for 8 h is 55.2 HV, which is 57.3% higher than the hardness value of the sample sintered for 2 h. In the literature, the hardness of pure Al was reported as 34 HV, and Al-CNT samples prepared by the powder metallurgy had hardness in the range of 32–50 HV [24].

The Al_2O_3 particles produced in the *in situ* reaction possess high hardness that can bear high pressure, so they contribute significantly to the hardness of the nanocomposite sintered for 8 h. On the other hand, MWCNTs and Al_2O_3 particles are dispersed in an entangled manner within the matrix, leading to increased dislocation density to prevent dislocation movement. Thus, the hardness of the nanocomposite is improved [25]. Moreover, as the reaction continues, the product Si is formed which grows gradually, leading to smaller matrix grains. According to Tabor equation where the composite hardness is given by Tabor [26],

$$\mathrm{HV} = \frac{\sigma_0 + Kd^{-0.5}}{3}, \tag{3}$$

where HV is the Vickers hardness, σ_0 is an inherent strength (MPa), K is a constant, and d is the grain size of the sample. Finer crystalline grains contribute to higher hardness of the nanocomposites.

Table 2: Mechanical property measurements of nanocomposites sintered for 2 h and 8 h, respectively.

Specimen	2 h		8 h	
	Average	Standard deviation	Average	Standard deviation
Hardness (HV)	35.1	2.1	55.2	3.1
Compressive strength (MPa)	265.2	24.2	334.1	17.9
Shear strength (MPa)	64.1	2.1	84.9	4.2

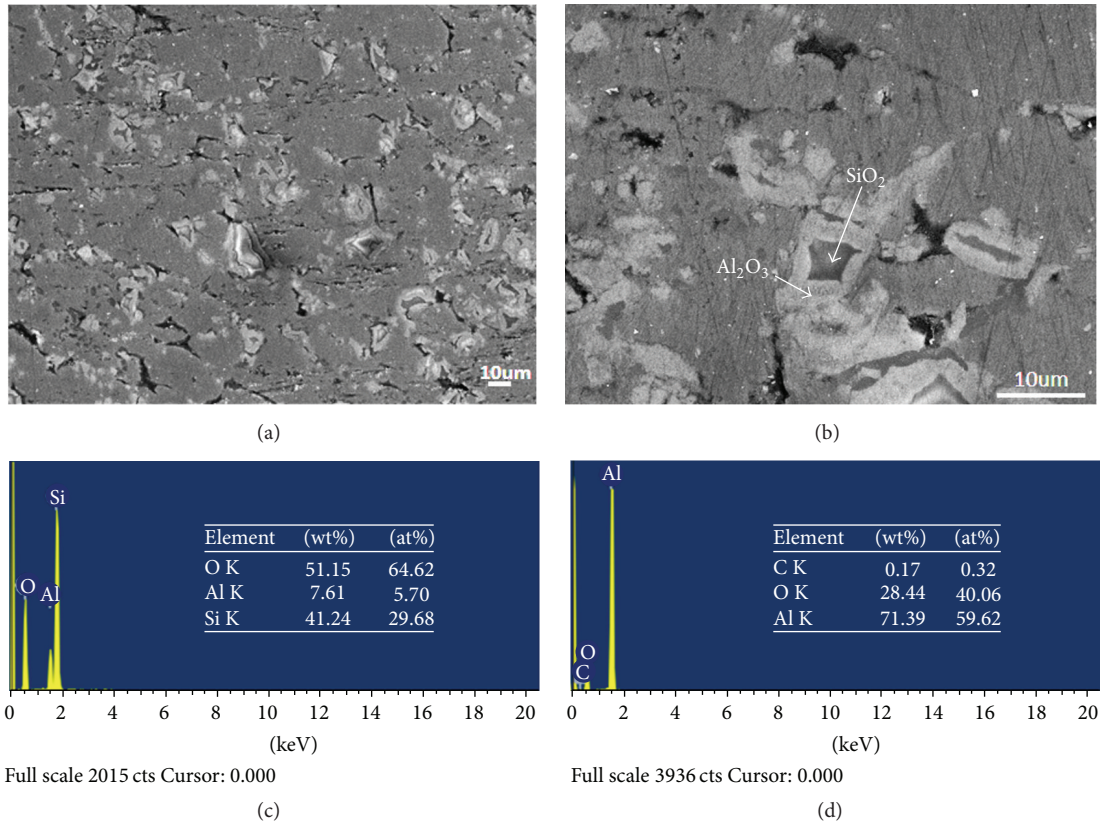

Figure 4: (a, b) SEM images of sintered nanocomposites with 8 h sintering time taken at a low magnification (a) and a higher magnification (b). (c) EDS from SiO_2; (d) EDS from Al_2O_3.

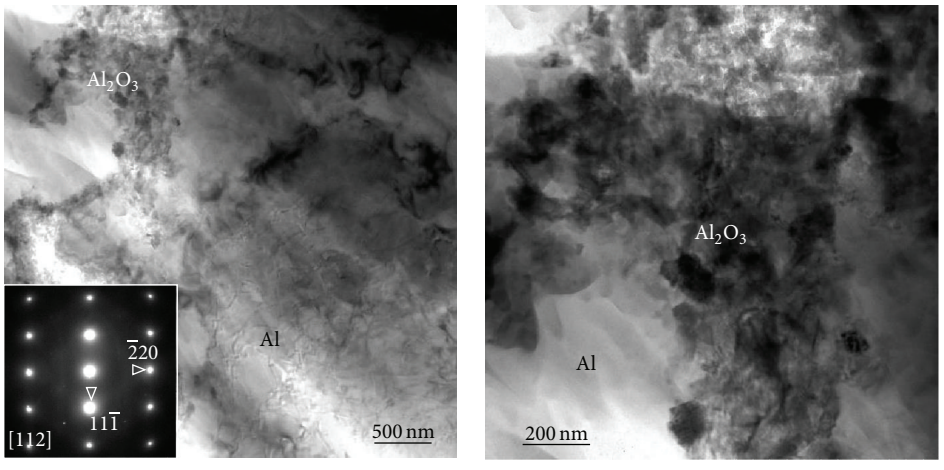

Figure 5: (a) TEM image showing high-density dislocations in Al (lower right) and Al_2O_3 particles (upper left); (b) magnified TEM image showing Al_2O_3. (a) is a diffraction pattern from the Al matrix.

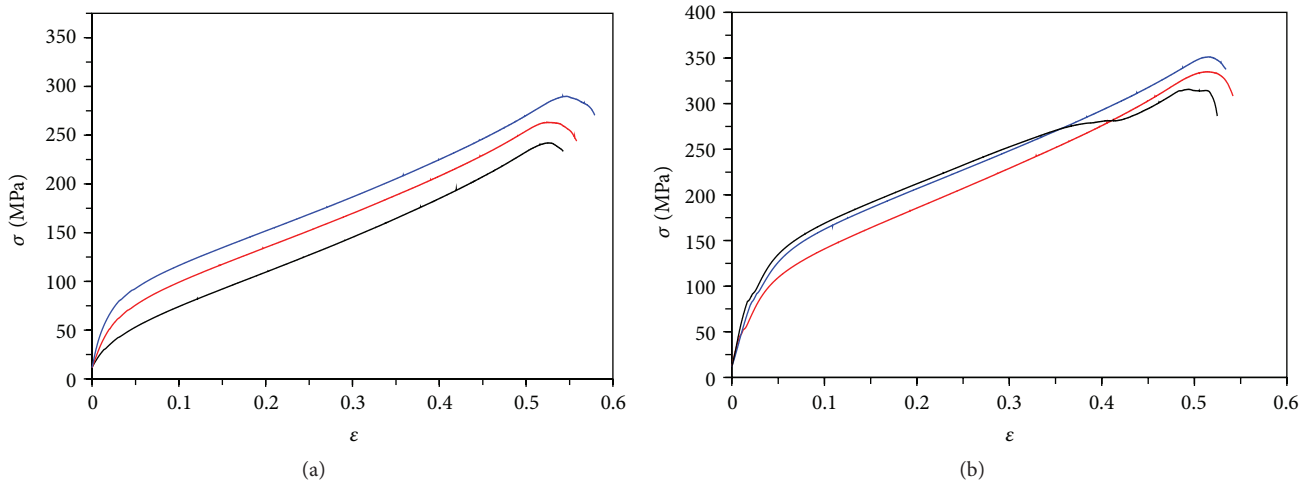

Figure 6: Compression deformation curves of nanocomposites sintered for 2 h (a) and 8 h (b).

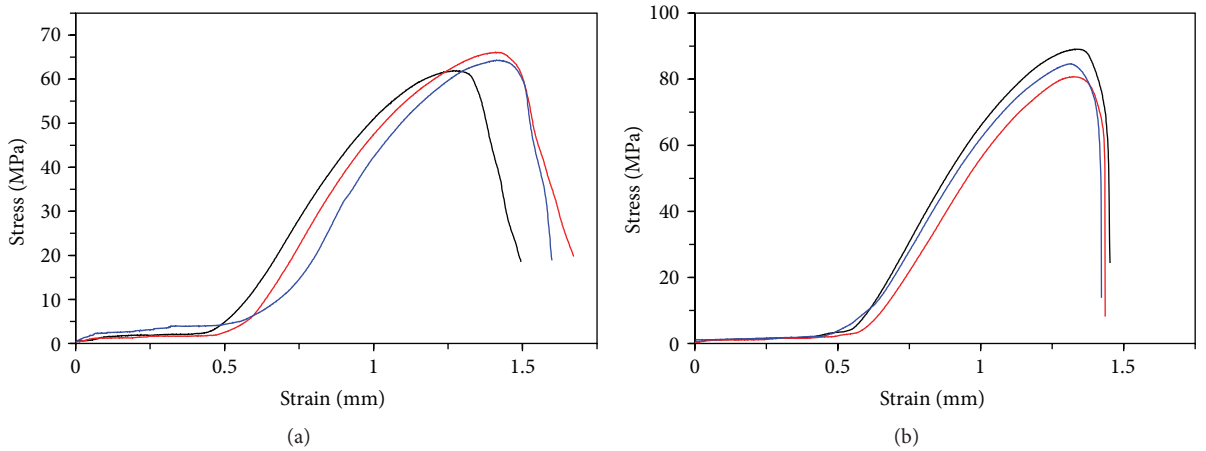

Figure 7: Shear deformation curves of nanocomposites sintered for 2 h (a) and 8 h (b).

3.3. Compressive Properties of the Nanocomposites. The compressive properties are listed in Table 2 and plotted in Figure 6, using three samples for each condition of 2 h and 8 h sintering time, respectively. The testing specimen fails with the increasing stress. Macrocracks, inclined at 45° to the axis, are present on the surface. In the beginning, a small portion of the stress-strain curve of the specimens exhibits a linear relationship, indicating the elastic deformation stage. Subsequently, the specimen enters a plastic deformation stage. The plastic deformation is not even, as MWCNTs and Al_2O_3 particles prevented the plastic flow of the Al matrix. As the deformation continues, the compressive capacity of the specimen improves gradually and the compression curve ascends constantly. The average compressive strength of the nanocomposite sintered for 8 h is 334.1 MPa, which is 26.0% higher than that of the specimens sintered for 2 h. In the nanocomposite, as MWCNTs and Al_2O_3 have different thermal expansion coefficients and elasticity moduli, a high-density dislocation zone is expected to form near MWCNTs and Al_2O_3 [17, 27–30]. The dislocation strengthening effect caused by MWCNTs and Al_2O_3 jointly (8 h specimen) is higher than that caused by MWCNTs alone in the 2 h specimen almost without alumina. In the loading process, the nanocomposite reinforced jointly by MWCNTs and Al_2O_3 has more bearing phases than the composite material reinforced by MWCNTs. The loads are transferred from the matrix to the reinforcing phases, enabling the nanocomposite to have better compression resistance properties.

3.4. Shear Strength and Fracture Analysis. The average shear strength of the nanocomposites sintered by 8 h sintering is 84.9 MPa, which is 32.4% higher than that of the nanocomposite sintered by 2 h, as listed in Table 2 and plotted in Figure 7. The strengthening effect caused by Al_2O_3 and MWCNTs jointly (8 h specimens) is evidently higher than that by MWCNTs alone (2 h specimens). Since the secondary phases of Al_2O_3 and MWCNTs are uniformly distributed in the Al matrix, dislocations have to bypass these particles by the Orowan mechanism or they are blocked in the front of these particles.

Figure 8 presents SEM and EDS analyses of the shear fractures of the nanocomposite sintered for 8 h. As shown

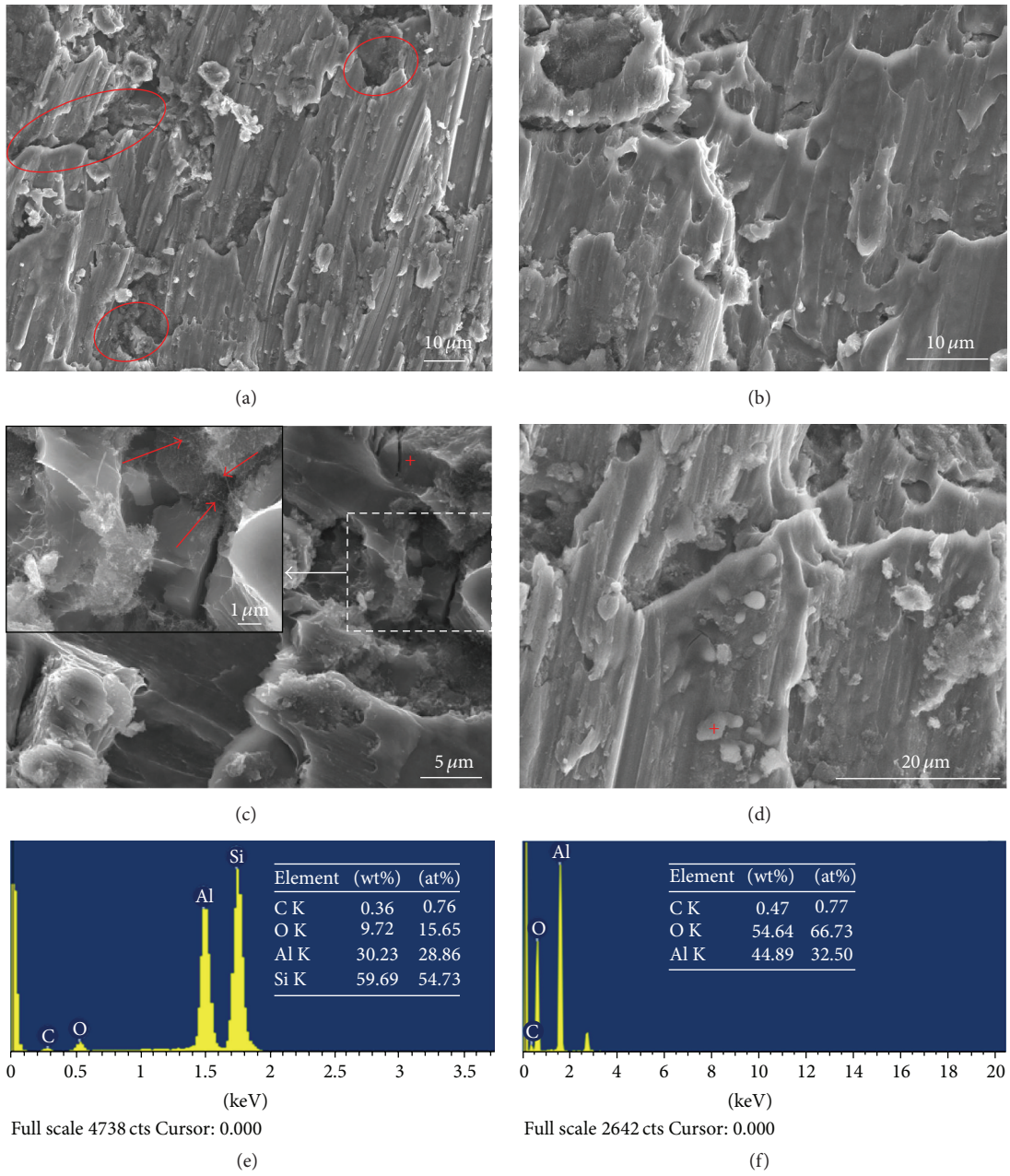

FIGURE 8: (a–d) SEM images of fractures of the nanocomposite. The EDS spectra in (e) and (f) are taken from the marked cross symbol spots in (c) and (d), respectively.

in Figure 8(a), since the nanocomposite is not completely densified, small cracks occur in the periphery of the pores under the external load, as circled in the figure. Dimple-shaped morphologies are observed in Figure 8(b), which are probably associated with the sites of secondary phases. Microcracks [31] a.e. present on the fracture surface, as shown in Figure 8(c). Based on the EDS in Figure 8(e), they are caused by transgranular fracture of Si which is a hard phase [32]. In addition, it is observed that partial CNTs are distributed on the interface on the fracture surface, as indicated by the arrows, which contribute to strengthening the nanocomposite during the load transfer [30, 33]. Figure 8(d) shows that the Al_2O_3 particles, as confirmed by EDS in Figure 8(f), are firmly bonded to the matrix, without evident signs of detachment under the external force. Therefore, the fracture mechanisms of the nanocomposite include microporous aggregation fractures of the matrix, interfacial debonding fractures, transgranular fractures of reinforcing particles, tears of matrix, and cracks of defects such as voids. The final failure of the material is a consequence of these fractures.

4. Conclusions

(1) Using a powder metallurgical *in situ* hot-pressing method, Al/Si/Al_2O_3/SiO_2/MWCNTs nanocomposites were sintered for a period of 8 h. The product alumina nanoparticles were found. However, the

sintering for 2 h yielded no evidence of the alumina phase by the *in situ* reaction.

(2) Micro-Vickers hardness value, compressive strength, and shear strength of the nanocomposite sintered for 8 h were measured to be 55.2 HV, 334.1 MPa, and 84.9 MPa, respectively, which were 57.3%, 26.0%, and 32.4% higher than those of the nanocomposite sintered for 2 h, due to the joint strengthening mechanism by Al_2O_3 and MWCNTs.

(3) Different fractures were observed in the nanocomposites, including microporous aggregation fractures of the matrix, interfacial debonding fractures, transgranular fractures of reinforcing particles, tears of matrix, and cracks of defects.

Conflict of Interests

The authors declare that there is no conflict of interests regarding the publication of this paper.

Acknowledgments

This work was supported by National Natural Science Foundation of China (no. 51201143), Fundamental Research Funds for the Central Universities (no. 2682015CX001), China Postdoctoral Science Foundation (no. 2015M570794), and Key Laboratory of Infrared Imaging Materials and Detectors, Shanghai Institute of Technical Physics, Chinese Academy of Sciences (no. IIMDKFJJ-14-04). Two of the coauthors (Shardai S. Johnson and Zhiping Luo) at FSU were supported by the U.S. NSF HRD-1436120, and the EPMA at FSU was funded by the U.S. DoD W911NF-09-1-0011. The TEM work was done at the Electron Microscopy Center at Argonne National Laboratory, which is operated by UChicago Argonne, LLC, under Contract DE-AC02-06CH11357.

References

[1] S. K. Singhal, R. Pasricha, M. Jangra, R. Chahal, S. Teotia, and R. B. Mathur, "Carbon nanotubes: amino functionalization and its application in the fabrication of Al-matrix composites," *Powder Technology*, vol. 215-216, no. 1, pp. 254–263, 2012.

[2] H. Kwon, M. Saarna, S. Yoon, A. Weidenkaff, and M. Leparoux, "Effect of milling time on dual-nanoparticulate-reinforced aluminum alloy matrix composite materials," *Materials Science and Engineering A*, vol. 590, no. 1, pp. 338–345, 2014.

[3] N. Saheb, Z. Iqbal, A. Khalil et al., "Spark plasma sintering of metals and metal matrix nanocomposites: a review," *Journal of Nanomaterials*, vol. 2012, Article ID 983470, 13 pages, 2012.

[4] J. B. Lu, Y. C. Mu, X. W. Luo, and J. T. Niu, "A new method for soldering particle-reinforced aluminum metal matrix composites," *Materials Science and Engineering B*, vol. 177, no. 20, pp. 1759–1763, 2012.

[5] H. G. Salem, S. El-Eskandarany, A. Kandil, and H. Abdul Fattah, "Bulk behavior of ball milled AA2124 nanostructured powders reinforced with TiC," *Journal of Nanomaterials*, vol. 2009, Article ID 479185, 12 pages, 2009.

[6] K. Dash, D. Chaira, and B. C. Ray, "Synthesis and characterization of aluminium-alumina micro-and nano-composites by spark plasma sintering," *Materials Research Bulletin*, vol. 48, no. 7, pp. 2535–2542, 2013.

[7] R. Casati, X. Wei, K. Xia et al., "Mechanical and functional properties of ultrafine grained Al wires reinforced by nano-Al_2O_3 particles," *Materials & Design*, vol. 64, no. 1, pp. 102–109, 2014.

[8] L. Jiang, Y.-Z. Cui, Y.-J. Shi, Y.-D. Ding, and F.-L. Yuan, "Preparation and mechanical properties of in situ Al_2O_3/Al composites by adding $NH_4AlO(OH)HCO_3$," *Transactions of Nonferrous Metals Society of China*, vol. 21, no. 10, pp. 2181–2185, 2011.

[9] T. Peng and I. Chang, "Mechanical alloying of multi-walled carbon nanotubes reinforced aluminum composite powder," *Powder Technology*, vol. 266, no. 1, pp. 7–15, 2014.

[10] H. Fukuda, K. Kondoh, J. Umeda, and B. Fugetsu, "Interfacial analysis between Mg matrix and carbon nanotubes in Mg-6 wt.% Al alloy matrix composites reinforced with carbon nanotubes," *Composites Science and Technology*, vol. 71, no. 5, pp. 705–709, 2011.

[11] X. D. Yang, E. Z. Liu, C. S. Shi et al., "Fabrication of carbon nanotube reinforced Al composites with well-balanced strength and ductility," *Journal of Alloys and Compounds*, vol. 563, no. 1, pp. 216–220, 2013.

[12] A. M. K. Esawi, K. Morsi, A. Sayed, M. Taher, and S. Lanka, "Effect of carbon nanotube (CNT) content on the mechanical properties of CNT-reinforced aluminium composites," *Composites Science and Technology*, vol. 70, no. 16, pp. 2237–2241, 2010.

[13] S. R. Bakshi and A. Agarwal, "An analysis of the factors affecting strengthening in carbon nanotube reinforced aluminum composites," *Carbon*, vol. 49, no. 2, pp. 533–544, 2011.

[14] Z. P. Luo and J. H. Koo, "Quantifying the dispersion of mixture microstructures," *Journal of Microscopy*, vol. 225, no. 2, pp. 118–125, 2007.

[15] Z. P. Luo, "Statistical quantification of the microstructural homogeneity of size and orientation distributions," *Journal of Materials Science*, vol. 45, no. 12, pp. 3228–3241, 2010.

[16] A. Baradeswaran and A. E. Perumal, "Study on mechanical and wear properties of Al 7075/Al_2O_3/graphite hybrid composites," *Composites Part B: Engineering*, vol. 56, no. 1, pp. 464–471, 2014.

[17] Y. Sun and H. Ahlatci, "Mechanical and wear behaviors of Al-12Si-*X*Mg composites reinforced with in situ Mg_2Si particles," *Materials & Design*, vol. 32, no. 5, pp. 2983–2987, 2011.

[18] W. Daoush, A. Francis, Y. Lin, and R. German, "An exploratory investigation on the in-situ synthesis of SiC/AlN/Al composites by spark plasma sintering," *Journal of Alloys and Compounds*, vol. 622, no. 2, pp. 458–462, 2015.

[19] Y. Huang, Q. B. Ouyang, D. Zhang, J. Zhu, R. X. Li, and H. Yu, "Carbon materials reinforced aluminum composites: a review," *Acta Metallurgica Sinica*, vol. 27, no. 5, pp. 775–786, 2014.

[20] J. R. Li, X. S. Jiang, R. Shen, Z. Y. Shao, D. G. Zhu, and D. Liu, "Dispersion characteristics of multi-walled carbon nanotubes and carbon nanoflakes with oxygen plasma," *Nanoscience and Nanotechnology Letters*, vol. 7, no. 7, pp. 581–587, 2015.

[21] X. S. Jiang, W. X. Liu, J. R. Li, Z. Y. Shao, and D. G. Zhu, "Microstructures and mechanical properties of Cu/Ti_3SiC_2/C/MWCNTs composites prepared by vacuum hot-pressing sintering," *Journal of Alloys and Compounds*, vol. 618, no. 1, pp. 700–706, 2015.

[22] S. K. Zhang, D. H. Wang, H. Zhao, and H. M. Miao, "The reaction between molten aluminum and silica glass," *Materials for Mechanical Engineering*, vol. 25, no. 1, p. 2830, 2001 (Chinese).

[23] H. G. Zhu, G. H. Guo, T. Cui, J. W. Huang, J. L. Li, and Z. H. Xie, "Influences of carbon additions on reaction mechanisms and tensile properties of Al-based composites synthesized *in-situ* by Al-SiO_2 powder system," *Materials Science and Engineering A*, vol. 623, no. 1, pp. 78–82, 2015.

[24] S. Simões, F. Viana, M. A. L. Reis, and M. F. Vieira, "Influence of dispersion/mixture time on mechanical properties of Al–CNTs nanocomposites," *Composite Structures*, vol. 126, no. 1, pp. 114–122, 2015.

[25] M. Naseri, A. Hassani, and M. Tajally, "Fabrication and characterization of hybrid composite strips with homogeneously dispersed ceramic particles by severe plastic deformation," *Ceramics International*, vol. 41, no. 3, pp. 3952–3960, 2015.

[26] C. R. Bradbury, J.-K. Gomon, L. Kollo, H. Kwon, and M. Leparoux, "Hardness of Multi Wall Carbon Nanotubes reinforced aluminium matrix composites," *Journal of Alloys and Compounds*, vol. 585, pp. 362–367, 2014.

[27] D. Lahiri, S. R. Bakshi, A. K. Keshri, Y. Liu, and A. Agarwal, "Dual strengthening mechanisms induced by carbon nanotubes in roll bonded aluminum composites," *Materials Science and Engineering A*, vol. 523, no. 1-2, pp. 263–270, 2009.

[28] R. George, K. T. Kashyap, R. Rahul, and S. Yamdagni, "Strengthening in carbon nanotube/aluminium (CNT/Al) composites," *Scripta Materialia*, vol. 53, no. 10, pp. 1159–1163, 2005.

[29] S. A. Sajjadi, H. R. Ezatpour, and H. Beygi, "Microstructure and mechanical properties of Al-Al_2O_3 micro and nano composites fabricated by stir casting," *Materials Science and Engineering A*, vol. 528, no. 29-30, pp. 8765–8771, 2011.

[30] C. D. Li, X. J. Wang, W. Q. Liu et al., "Microstructure and strengthening mechanism of carbon nanotubes reinforced magnesium matrix composite," *Materials Science and Engineering A*, vol. 597, no. 1, pp. 264–269, 2014.

[31] H. Abdizadeh and M. A. Baghchesara, "Investigation on mechanical properties and fracture behavior of A356 aluminum alloy based ZrO_2 particle reinforced metal-matrix composites," *Ceramics International*, vol. 39, no. 2, pp. 2045–2050, 2013.

[32] H. G. Zhu, K. Dong, J. W. Huang, J. L. Li, G. Wang, and Z. H. Xie, "Reaction mechanism and mechanical properties of an aluminum-based composite fabricated in-situ from Al-SiO_2 system," *Materials Chemistry and Physics*, vol. 145, no. 3, pp. 334–341, 2014.

[33] X. Zhou, D. P. Su, C. W. Wu, and L. M. Liu, "Tensile mechanical properties and strengthening mechanism of hybrid carbon nanotube and silicon carbide nanoparticle-reinforced magnesium alloy composites," *Journal of Nanomaterials*, vol. 2012, Article ID 851862, 7 pages, 2012.